Journal of Materials Chemistry B

Silicone-containing thermoresponsive membranes to form an optical glucose biosensor

Journal:	*Journal of Materials Chemistry B*
Manuscript ID	TB-ART-06-2022-001192.R1
Article Type:	Paper
Date Submitted by the Author:	17-Jul-2022
Complete List of Authors:	Dong, Ping; Texas A&M University, Biomedical Engineering Singh, Kanwar Abhay; Texas A&M University, Department of Biomedical Engineering Soltes, Amelia; Texas A&M University, Biomedical Engineering Ko, Brian; Texas A&M University, Biomedical Engineering Gaharwar, Akhilesh; Texas A&M University, Department of Biomedical Engineering; Texas A&M University, Center for Remote Health Technologies Systems; Texas A&M University, Interdisciplinary Program in Genetics and Genomics McShane, Michael J.; Texas A&M University, Biomedical Engineering; Texas A&M University, Materials Science & Engineering; Texas A&M University, Center for Remote Health Technologies Systems Grunlan, Melissa; Texas A&M University System, Biomedical Engineering; Texas A&M University, Materials Science & Engineering; Texas A&M University, Chemistry; Texas A&M University, Center for Remote Health Technologies Systems

Silicone-containing thermoresponsive membranes to form an optical glucose biosensor

Ping Dong,[†] Kanwar Abhay Singh,[†] Amelia M. Soltes,[†] Brian S. Ko,[†] Akhilesh K. Gaharwar,[†,‖,$] Michael J. McShane,[†,‡,‖] Melissa A. Grunlan*[†,‡,§,‖]

[†]Department of Biomedical Engineering, Texas A&M University, College Station, TX 77843-3120 (USA)

[‡]Department of Materials Science & Engineering, Texas A&M University, College Station, TX 77843-3003 (USA)

[$]Interdisciplinary Program in Genetics and Genomics, Texas A&M University, College Station, TX 77843 (USA).

[§]Department of Chemistry, Texas A&M University, College Station, TX 77843-3120 (USA)

[‖]Center for Remote Health Technologies Systems, Texas A&M University, College Station, TX 77843-3120 (USA)

*E-mail: mgrunlan@tamu.edu

Keywords: glucose biosensor, thermoresponsive, double network, hydrogel

Abstract

Glucose biosensors that could be subcutaneously injected and interrogated without a physically connected electrode and transmitter affixed to skin would represent a major advancement in reducing the user burden of continuous glucose monitors (CGMs). Towards this goal, an optical

glucose biosensor was formed by strategically tailoring a thermoresponsive double network (DN) membrane to house a phosphorescence lifetime-based glucose sensing assay. This membrane was selected based on its potential to exhibit reduced biofouling via 'self-cleaning' due to cyclical deswelling/reswelling *in vivo*. The membrane was strategically tailored to incorporate oxygen-sensitive metalloporphyrin phosphor, Pd meso-tetra(sulfophenyl)-tetrabenzoporphyrin ($[PdPh_4(SO_3Na)_4TBP]_3$) (HULK) and glucose oxidase (GOx). Specifically, electrostatic and hydrophobic interactions were used to stabilize HULK and GOx within the membrane, respectively. Enhancing the oxygen permeability of the membrane was necessary to achieve sensitivity of HULK/GOx to physiological glucose levels. Thus, silicone microparticles were incorporated at two concentrations. Key properties of *SiHy*-0.25 and *SiHy*-0.5 microparticle-containing compositions were compared to a control having no microparticles (*SiHy*-0). The discrete nature of the silicone microparticles maintained the desired thermosensitivity profile and did not impact water content. While the modulus decreased with silicone microparticle content, membranes were more mechanically robust versus a conventional hydrogel. *SiHy*-0.25, owing to apparent phase separation, displayed greater glucose diffusion and oxygen permeability versus *SiHy*-0.5. Furthermore, *SiHy*-0.25 biosensors exhibited the greatest glucose sensitivity range of 100 to 300 mg/dL versus only 100 to 150 mg/dL for both *SiHy*-0 and *SiHy*-0.5 biosensors.

Introduction

As the prevalence of diabetes increases,[1-5] continuous glucose monitors (CGMs) have emerged to permit real-time tracking of glucose levels for improved blood sugar management and subsequent reduction of short- and long-term complications.[6-11] On-the-market CGMs (Medtronic Guardian™, Dexcom G6, and Abbott FreeStyle® Libre 2) employ a transcutaneous electrochemical sensor

designed for monitoring glucose levels in the interstitial fluid (ISF). The transcutaneous probe is linked to a transmitter that is adhered to the skin on the upper arm or abdomen, and delivers the data to a customized reader or a smart phone. While improvements have been made related to the probe (e.g., ease of insertion, and reduced irritation and infections),[12] biofouling necessitates frequent replacements (~7-14 days), leading to inconvenience, recurring costs, and the potential for subcutaneous fibroses.[11, 13-15] Anticipated to improve comfort and convenience, Senseonics developed a CGM (Eversense®) based on a subcutaneous implant (d ~3.5 mm × l ~ 18.3 mm) that contains an optical hydrogel sensor, optics, and electronics enclosed in a poly(methyl methacrylate) (PMMA) cylinder case and utilizes a silicone collar to release anti-inflammatory dexamethasone acetate.[16-17] The current version of this device (Eversense® E3) was recently approved by the FDA for non-adjunctive, decision-making use up to six months in patients ≥18 years of age.[18] However, some significant drawbacks of this CGM include the need for surgical implantation and removal (in the upper arm), as well as the relatively bulky affixed external transmitter.

Realizing a glucose biosensor small enough to be non-surgically inserted (e.g., injected) into the subcutaneous tissue (e.g., via trocar needle), interrogated without a skin-attached transmitter, and able to function for extended periods requires overcoming significant challenges. Optical glucose sensors offer advantages over electrochemical sensors as they may be interrogated exclusively via a LED and photodiode pair on a smartwatch or other simple wearable, allowing for the elimination of skin-attached transmitters. Numerous optical glucose sensing approaches have been studied,[13, 19-21] including those employing assays based on luminescence measurements (e.g., Förster resonance energy transfer [FRET)] assays,[22-27] phenylboronic fluorescence assays,[28-29] and phosphorescence lifetime assays[30]). To advance the design of an optical glucose biosensor, the way the assay is housed is paramount in determining success. The design must address numerous issues,

including ease of biosensor fabrication, assay retention, glucose diffusion to the assay, and minimizing surface biofouling and the foreign body reaction (FBR). This latter issue is considered the most significant barrier to the long-term functionality of implanted glucose biosensors.[22-27] Numerous material strategies have been explored to improve implant biocompatibility, including refining implant shape, size and stiffness,[31-33] anti-inflammatory drug elution,[34-35] and surface modifications.[36-38] Owing to the tunability of diffusivity, permeability, and other key properties, hydrogels have emerged as particularly intriguing options for constructing glucose biosensors,[28, 39] as both surface coatings [38, 40-41] as well as bulk matrices to embed assays.[28, 42]

Herein, we report the proof-of-concept study of an optical glucose biosensor constructed from a phosphorescence lifetime assay embedded in a customized thermoresponsive membrane. The assay is based on an oxygen-sensitive metalloporphyrin phosphor, Pd meso-tetra(sulfophenyl)-tetrabenzoporphyrin ($[PdPh_4(SO_3Na)_4TBP]_3$) (denoted by us as "HULK" for its bright green color) in combination with glucose oxidase (GOx).[30, 43-48] The combination of HULK and GOx provides distinct advantages versus other glucose-sensitive assays based on fluorescence intensity, due to the high selectivity and sensitivity of the enzymatic reaction as well as factors that impact fluorophores (e.g., photo-bleaching[28, 44, 47]) and attenuate excitation signals (e.g., skin thickness or tone).[49-51] In the case of HULK, phosphorescence lifetime is regulated by collisional quenching by oxygen, such that increased oxygen levels lead to a decreased lifetime; lifetime changes are proportional to intensity changes but are independent of the assay concentration, excitation source intensity, or other environmental factors.[45, 52-53] When combined with an oxidoreductase enzyme, phosphorescence intensity or lifetime measurements can be used to indirectly monitor enzymatic substrate concentrations. Specifically, per Equation 1, the phosphorescence intensity/lifetime of HULK can be related to glucose levels as oxygen is consumed via glucose oxidation as catalyzed

by GOx.

$$\beta\text{-D-Glucose} + O_2 + H_2O \xrightarrow{GOx} D\text{-}Glucono\text{-}1,5\text{-}Lactone + H_2O_2 \qquad (1)$$

In terms of the membrane used to house the HULK/GOx assay for use in contact with biological tissues and fluids, a primary consideration is the expected biofouling following implantation. In contrast to typical strategies employing passive resistance to biofouling,[25, 54-55] we have previously reported a thermoresponsive, "self-cleaning" double network (DN) hydrogel membrane with excellent biocompatibility.[56] Based on thermoresponsive *N*-isopropylacrylamide (NIPAAm) and anionic 2-acrylamido-2-methylpropane sulfonic acid (AMPS), the membrane was comprised of a tightly crosslinked 1st network of [P(NIPAAm-*co*-AMPS)] (75:25 wt% ratio), and a loosely crosslinked 2nd network of NIPAAm copolymerized with hydrophilic *N*-vinylpyrrolidone (NVP) to precisely tune the volume phase transition temperature (VPTT). Thus, the membrane's VPTT could be tailored to produce cyclical deswelling/reswelling with temperature fluctuations occurring in subcutaneous tissues, for both rat models (~37-38 ºC)[57-58] and the human wrist (~35-36 ºC).[59-60] Implant-sized cylindrical membranes (*d*~2.5 x *l*~5 mm) were shown to intermittently and slightly deswell (Δd ~20-25 μm) at these relatively higher temperatures. This active "self-cleaning" was predicted to prevent cellular adhesion *in vivo*, as was observed for cells cultured on similar thermoresponsive hydrogels.[61] Moreover, following 90 days in a subcutaneous rat model, these implant-size membranes (VPTT profile: T_{onset} ~36.5 °C, T_{max} of ~39 °C) exhibited excellent biocompatibility with a fast healing response and a remarkably thin fibrous capsule.[56]

A new, customized thermoresponsive membrane is required for effective incorporation of the HULK and GOx assay components and glucose sensitivity. In our recent report, a distinct DN hydrogel membrane was prepared to leverage electrostatic interactions and covalent bonding with

the assay components.[62] This membrane was based on a NIPAAm and cationic (3-acrylamidopropyl) trimethylammonium chloride at 75:25 mol% 1st network [P(NIPAAm-*co*-APTAC)] and loosely crosslinked NIPAAm and acrylamide 2nd network [P(NIPAAm-*co*-AAm)]. The VPTT was precisely tuned with AAm to afford the aforementioned targeted VPTT profile. During formation of the cationic 1st network, the anionic HULK was incorporated to leverage electrostatic interactions for its retention. GOx was introduced along with glutaraldehyde during formation of the 2nd network, permitting covalent bonding of GOx with AAm segments' primary amides, as well as with dialdehydes of glutaraldehyde. As a result, the HULK and GOx were successfully immobilized within the membrane, and the resulting biosensor achieved sensitivity for glucose levels from 50 up to 200 mg/dL, representing efficacy in the hypoglycemic (<70 mg/dL) to normal (70-130 mg/dL) and slightly elevated physiological glycemic ranges. The lack of sensitivity at higher glucose levels (i.e., 200-500 mg/dL or "hyperglycemic") was attributed to a sub-optimal oxygen permeability of the membrane relative the glucose supply rate, leading to oxygen depletion. For oxygen-sensitive HULK/GOx glucose sensing, membrane oxygen levels are critical (Scheme 1a). Because the oxygen concentration directly influences the resulting phosphorescence intensity, three possible scenarios may occur within the physiological glucose concentration range (50 - 500 mg/dL) (Scheme 1b). Two of these scenarios would not yield the desired differences in phosphorescence intensity: (i) if membrane oxygen permeability is very low relative to oxygen consumption ("oxygen consumption dominant"), and (ii) if membrane oxygen permeability is very high relative to oxygen consumption ("oxygen diffusion dominant"). These result in sensitivity to glucose that is too high and too low for, respectively, to make reliable measurements over the target range of glucose concentrations. The third and ideal scenario would occur when membrane oxygen permeability affords sufficient oxygen levels ("oxygen sufficiently

supplied"), resulting in an appropriate balance of oxygen supply and consumption to yield sensitive response over the desired glucose range.

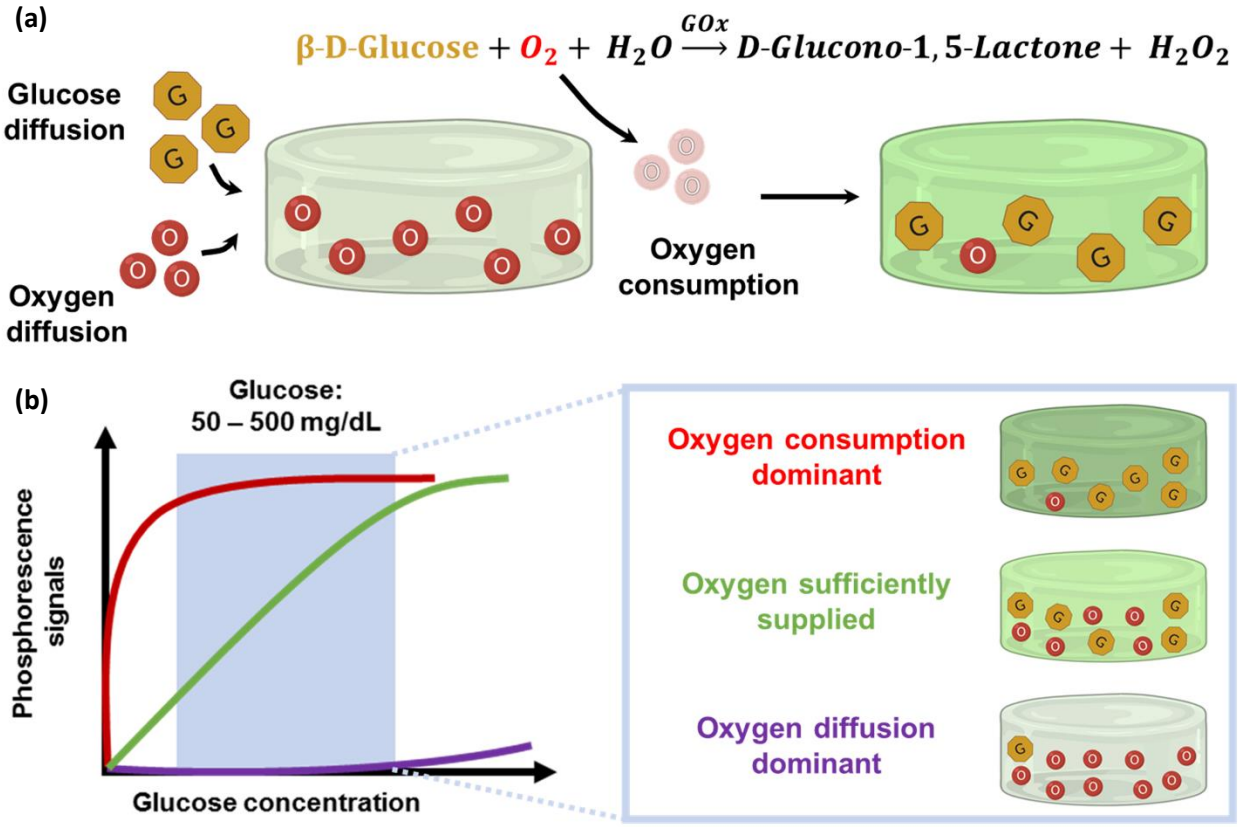

Scheme 1. (a) Sensing mechanism of HULK/GOx embedded in a membrane. With increased glucose levels, more oxygen in the membrane is consumed via glucose oxidation, resulting in increased phosphorescence intensity/lifetime. Thus, the phosphorescence intensity/lifetime is directly related to the oxygen concentration in the membrane, which is in turn determined by the membrane's oxygen permeability and oxygen consumption. (b) Three possible general scenarios related to membrane oxygen levels and the phosphorescence intensity/lifetime relationship with increasing glucose levels in the physiological glucose range (50 - 500 mg/dL); "oxygen sufficiently supplied" provides the desired sensitivity over the range of interest.

Thus, to produce the desired sensitivity of HULK/GOx to physiological glucose levels, the oxygen permeability of the thermoresponsive membrane must be enhanced. Herein, to achieve this, membranes were modified with silicone microdomains. Polydimethylsiloxane (PDMS) has been incorporated into various hydrogels to improve gas permeability,[63-64] related to the flexibility of

chains comprised of siloxane bonds that yield increased free volume for diffusion.[65-69] Due to the insolubility of PDMS in aqueous solution, the manner of incorporation is imperative to achieve good distribution within the membrane. To modify the 1st network precursor solution, an ultrasonication processor was used to disperse the silicone phase, consisting of 3-(methacryloyloxy)propyltris(trimethylsiloxy)silane (TRIS), methacryloxypropyl terminated polydimethylsiloxane (PDMS) (DMS-R05), and a photoinitiator. The resulting emulsion was UV-cured, producing a 1st network [P(NIPAAm-*co*-APTAC)] with embedded silicone microparticles. The P(NIPAAm-*co*-AAm) 2nd network was subsequently formed. Membranes were formed with different concentrations of silicone microdroplets, denoted as "*SiHy*-x", where x = TRIS concentration (x = 0, 0.25 or 0.5 M) in the 1st network precursor solution. These were characterized in terms of key material properties, such as VPTT profile, glucose diffusivity, and mechanical properties. HULK and GOx were incorporated into the DN membranes at different concentrations, and the phosphorescent properties were related to glucose levels.

Experimental

Materials. 3-(Methacryloyloxy)propyltris(trimethylsiloxy)silane (TRIS) was purchased from Alfa Aesar. Methacryloxypropyl-terminated polydimethylsiloxane (4-6 cSt, DMS-R05) was purchased from Gelest. (3-Acrylamidopropyl)trimethylammonium chloride solution (75% wt.% in water, APTAC), *N*-isopropylacrylamide (97%, NIPAAm), *N*,*N*'-methylenebisacrylamide (99%, BIS), 2-hydroxy-4'-(2-hydroxyethoxy)-2-methylpropiophenone (98%, Irgacure 2959, "Irg"), acrylamide (≥ 99%, AAm), 2-hydroxy-2-methylpropiophenone (97%, Darocur® 1173), poly(vinyl alcohol) (PVA) (87-90% hydrolyzed, M_w ~30-70 kg/mol), ethanol (HPLC grade), Triton™ X-100 (laboratory grade), glucose oxidase (GOx) (100k - 250k units/g solid, without added oxygen), and glutaraldehyde solution (Grade II, 25% in water) were obtained from Sigma-Aldrich. Mouse

fibroblast cells (NIH/3T3) were obtained from the American Type Culture Collection (ATCC). Dulbecco's Modified Eagle's Medium (DMEM, HyClone, GE Sciences), phosphate-buffered saline (PBS, 1X, pH 7.4, without calcium and magnesium, Corning®) and trypsin-EDTA (0.5%, no phenol red, Gibco) were purchased from Fisher Scientific. Fetal bovine serum (FBS; Atlanta Biologicals, USA), and penicillin/streptomycin (100 U/100 µg/mL, Gibco), alamarBlue™, phalloidin stain (Biotium) and Hoechst 33258 (Biotium) were obtained from Thermo Fisher. All chemicals were used directly without further purification. Deionized water (DI) with a resistance of 18 MΩ·cm was purified with Cascada LS MK2 (Pall).

Membrane Fabrication. The DN membranes were fabricated via a 2-step UV-curing process **(Scheme 2, Table 1)**. The membrane compositions were denoted as *SiHy*-x (x = 0, 0.25 or 0.5), where *x* represents the molar concentrations of TRIS used in the formation of the 1st network. Thus, *SiHy-0* served as a "silicone-free" control. A single network (SN) (i.e., 1st network) precursor solution (for *SiHy-0*) or emulsions (for *SiHy-0.25* and *SiHy-0.5*) was prepared in in 2 steps. First, an "aqueous phase" was prepared by combining NIPAAm, APTAC, crosslinker (BIS, 2.5 mol% based on NIPAAm and APTAC concentration), and photoinitiator (Irgacure 2959, 0.5 mol% based on NIPAAm and APTAC concentration) in a 1 % (wt/vol) PVA aqueous solution. For *SiHy-0.25* and *SiHy-0.5,* a "silicone phase" was then prepared by combining TRIS, DMS-R05 (2.5 mol% based on TRIS), and Darocur 1173 (0.5 mol% based on TRIS). The silicone and aqueous phases were combined and subjected to an ultrasonic processor (Fisher Scientific, 120 Watt, 20 kHz), with 30% amplitude for 5 min. The resulting solution or emulsion was immediately injected into a rectangular mold assembled by clipping a silicone spacer (t ~0.7 mm or ~0.2 mm) between two glass slides (75 × 55 mm). While submerged in an ice-water bath, the mold was exposed to a UV lamp (UV-transilluminator, 6 mW/cm^2, λ_{peak} = 365 nm) for 60 min (rotating the side facing down

upwards after 30 min). The resulting SN was removed from the mold, and immediately soaked in the 2nd network precursor solution for 24 hr in a ~5 ºC refrigerator. The 2nd network solution was

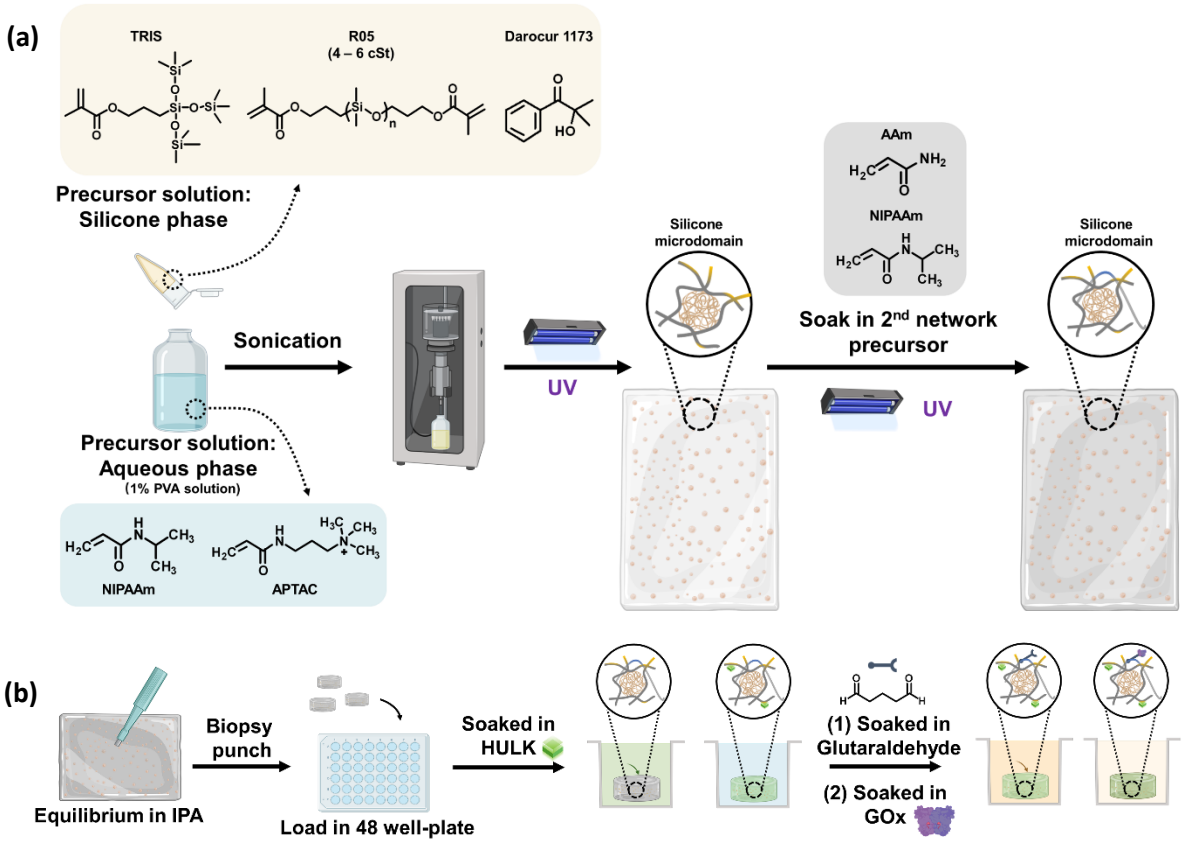

Scheme 2. (a) Fabrication of thermoresponsive DN hydrogels containing the silicone microdomains. (b) Incorporation of HULK and GOx into membrane.

Table 1. Compositions, VPTTs, and water contents of DN membranes prepared with different concentrations of a silicone microdomain phase.

	1st network (1 M)			2nd network		DN		
	Aqueous Phase		Silicone Phase	Monomer		VPTT		Water content
	NIPAAm	APTAC	TRIS	NIPAAm	AAm	T_o	T_{max}	
SiHy-0	0.75 M	0.25 M	0 M	2 M	5%	36.4 ± 0.2	38.5 ± 0.1	87.7 ± 0.3%
SiHy-0.25	0.5 M	0.25 M	0.25 M	2 M	5%	36.4 ± 0.2	38.4 ± 0.3	88.6 ± 0.4%
SiHy-0.5	0.25 M	0.25 M	0.5 M	2 M	5%	36.5 ± 0.2	38.1 ± 0.3	88.9 ± 0.2%

DN membranes were denoted as "*SiHy-x*", where *x* = TRIS concentration (i.e., 0, 0.25 or 0.5 M) in the 1st network precursor solution. BIS (2.5 mol% based on monomer concentration in aqueous phase) and Irg (0.5 mol% based on monomer concentration in aqueous phase) were added in the aqueous phase as crosslinker (BIS) and photoinitiator. For the silicone phase, DMS-R05 (2.5 mol% based on TRIS concentration) and Darocur 1173 (0.5 mol% based on TRIS concentration) were added as crosslinker and photoinitiator. The 2nd network was consisted of 5 wt% of AAm in addition to 2M NIPAAm, 0.1 mol% of BIS based on NIPAAm, and 2 mol% of Irg 2959 based on NIPAAm.

prepared with 2 M NIPAAm, 5 wt% AAm (based on NIPAAm), 0.1 mol% of BIS (based on NIPAAm), and 2 mol% of Irg 2959 (based on NIPAAm) dissolved in DI water. Following soaking in the 2nd network precursor solution, the membrane was placed in a sandwich mold assembled with a polycarbonate spacer (t ~1 mm or ~0.25 mm) in between two glass slides (75 mm × 50 mm). The mold was immersed in an ice-water bath while subjecting to UV-curing for 60 min (rotating the side facing down upwards after 30 min). The resulting DN membranes were sequentially immersed in 100% IPA for 2 days and DI for 2 days, with media changes every 12 hr. The thicker DN membrane specimens (t ~ 1.2 mm) (i.e., prepared with 1 mm 2nd spacer) were utilized to characterize the membrane physical properties. The thinner DN membrane specimens (t ~ 0.5 mm) (i.e., prepared with 0.25 mm 2nd spacer) were utilized for glucose sensor fabrication.

Characterization of silicone phase microdroplet size in emulsions. The 1st network precursor emulsion (*SiHy*-0.25 or *SiHy*-0.5) was diluted 100X with 1 % (wt/vol) PVA solution. A drop of the diluted solution (0.5 μL) was vacuum dried (30 in. Hg) on an aluminum specimen mount (d ~12.7 mm, Electron Microscopy Sciences) at room temperature (RT). The dried samples were subjected to Au-Pt sputter coating (~ 7 nm) and imaged with a scanning electron microscope (SEM, Tecan Vega 3, accelerating voltage of 10 kV). Image analysis software (Image J) was used to analyze the size of the microdroplets. Measurements (N = 20) were taken along the two diagonal midlines of each SEM image (N = 5 per composition).

Sol Content. SN and DN disc specimens (SN: t ~0.7 mm; DN: t ~1 mm) were harvested via biopsy punch from slabs immediately after curing (N = 5, d ~8 mm), and were vacuum dried overnight (ON) (RT, 30 in. Hg) to obtain the original dry weight (W_{d0}). Disc specimens were then sequentially immersed in 20 mL of 100% IPA for 2 days and 20 mL of DI for 2 days, with media changing every 12 hr. Next, the disc specimens were vacuum dried ON (RT, 30 in. Hg) to obtain

the dry weight following equilibration in solvents (W_{d1}). The sol content for specimens were calculated per Equation 2:

$$\text{Sol content} = \frac{W_{d0} - W_{d1}}{W_{d0}} \times 100\% \quad (2)$$

Volume phase transition temperature (VPTT). The VPTT of DN membranes was measured using differential scanning calorimetry (DSC, TA Instruments Q100). A small piece (~10 mg, N = 3) was harvested from a swollen membrane (t ~1.2 mm) with razor blade, blotted with a Kimwipe, and then sealed in a hermetic pan. Following cooling to 0 ºC, specimens were heated to 60 ºC at a rate of 3 ºC/min for 2 cycles. The VPTT was reported with onset temperature of the endothermic phase transition (T_o) and the peak temperature (T_{max}) of the transition. All the results reported were from the 2nd cycle to remove any thermal history.

Equilibrium water Content. Disc specimens (d ~8 mm × t ~1.2 mm, N = 5) were harvested from a swollen DN membrane slabs with a biopsy punch. Each disc was equilibrated in 20 mL DI for 24 hr (RT). Upon removal, the discs were blotted with Kimwipes and weighed on a digital scale (swollen weight, W_s). The swollen discs were subsequently vacuum dried ON (RT, 30 in. Hg) to obtain the dry weight (W_d). The water content (W_c) was defined per Equation 3:

$$W_c = \frac{W_s - W_d}{W_s} \times 100\% \quad (3)$$

Attenuated total reflectance-Fourier transform infrared spectroscopy (ATR-FTIR). Disc samples (N = 3, d ~8 mm) were punched from DN membranes slabs and were vacuum dried (30 in. Hg) under RT. ATR-FTIR (Bruker ALPHA-Platinum, N = 32) were used to confirm the peaks of Si-CH_3 (1280 – 1240 nm), Si-O-Si (1100 – 1000 nm), and Si-$(CH_3)_2$ (840 – 790 nm).

Morphology. SEM (Tecan Vega 3, accelerating voltage of 10 kV) was used to observe the cross-section morphology of the membranes. A small piece was harvested from a DN membrane slab

with a razor blade, cutting off a thin layer on both top and bottom exposing the cross-section. The samples were vacuum dried ON (RT, 30 in. Hg) and were sputter coated with Au-Pt (~ 7 nm) prior to imaging. SEM (Tecan Vega 3) with Oxford energy-dispersive x-ray spectroscopy (EDS) detector was used to analysis the elements on membrane cross-sections. Five random points were selected for the EDS scanning and the average elements concentration at those points were calculated.

Confocal laser scanning microscopy (CLSM) Representative DN membrane disc samples (d ~8 mm × t ~1.2 mm, $N = 1$) were harvested with a biopsy punch and were stained with Nile Red solution for 24 hr. A Nile red solution was prepared by dilute 75 µL of 20 mg/mL Nile red methanol solution with 128 mL of DI.[70] An Olympus FV1000 confocal microscope was used to image each sample (excitation: 488 nm and emission: 500–600 nm). Z-stack images were acquired with a 0.53 µm/slice for 20 µm depth. Representative slices of the stacks were exported without pseudo-color.

Hydrophilicity. Surface hydrophilicity of the DN membrane slabs was characterized via static water contact angle (θ_{static}) with a CAM-200 goniometer (KSV instruments) equipped with an autodispenser, video camera and drop-shape analysis software (Attention Theta). A 5 µL DI droplet was placed on the surface of a membrane (blotted with Kim Wipes) and the θ_{static} was monitored over 1 min. The θ_{static} ($N = 5$) at 0 min and 1 min were compared through all compositions.

The bulk hydrophilicity of DNs was evaluated by determination of H-index.[71] Disc samples ($N = 10$, d ~8 mm, t ~1.2 mm) were harvested from DN membranes and were vacuum dried (30 in. Hg, RT, ON) for dry weight (W_d). Those discs were submerged in 20 mL of 70% IPA ($N = 5$) or 100% DI ($N = 5$) for 24 hr. The swollen weight (W_s) of each disc was measured and the equilibrium swollen ratio ($Q = W_s/W_d$) was calculated for either swollen in 100% DI (Q_{DI}) or 70% IPA (Q_{IPA}). The H-index (H) was defined as Q_{IPA}/Q_{DI}.

Mechanical properties. Compression tests were performed with an Instron 5944 at RT. DN

membrane disc specimens (d ~6 mm × t ~1.2 mm, *N* = 5) were harvested with biopsy punches and blotted with Kimwipes prior to tests. Each disc was placed at the center of the bottom platen and was subjected to a 0.5 N pre-load force, following with compression at a constant strain rate (1 mm/min) until fracture (force drop > 0.5 N). The compressive modulus was calculated from the linear portion of the strain-stress curve (from 0 to 10% strain). The compressive strength and the compressive strain were determined at the point of fracture.

Glucose diffusion coefficient. DN membrane slabs were cut into square shapes (d ~15 mm × t ~1.2 mm; *N* = 3 from different DN slabs) with a single edge razor blade. Each sample was placed and gently clamped between two side-by-side diffusion chambers with 1.5cm diameter orifice (PermeGear). DI water (7 mL) and glucose solution (7 mL, 10 mg/mL) were added into the receiver and donor chambers, respectively. Each chamber was stirred with a Teflon-coated stir bar at 100 rpm to maintain a homogenous solution. The solution temperature was maintained at RT (22 ºC) or 37 °C with the water heating jacket system. At 10 min intervals over a period of 1.5 hr, 50 μL of solution was collected from each chamber. Afterward, glucose concentration of individual collected solution was measured with YSI (YSI 2700 Select Biochemistry Analyzer).

Fick's law was used to calculate the diffusion coefficient (D_{eff}) of glucose passing through a hydrogel membrane.[72-73] Equation 4 was used for a side-by-side diffusion model. [Q: quantity of glucose transferred, t: time interval of the diffusion, L: thickness of the sample (~1.2 mm), C_o: the initial glucose concentration (10 mg/mL) and A: the area of the samples exposing for diffusion (1.767 cm^2)]

$$Q = \frac{ADC_0}{L} \times (t - \frac{L^2}{6D_{eff}}) \quad (4)$$

Fabrication of HULK-containing DN membranes. As illustrated in Scheme 2b, disc samples

were harvested from hydrogel slabs (t ~0.5 mm) using a 6 mm biopsy punch. Each sample (d ~6 mm, t ~0.5 mm) was immersed in 300 μL of 0.1 mM HULK solution (in IPA) for 48 hr at 35 °C. After soaking, each disc was washed with DI (1 mL, 3 × 10 min) and equilibrated in DI water ON.

According to the Beer-Lambert Law,[74] the actual concentration of HULK incorporated into a DN membrane should follow a linear relationship with the membrane's absorbance. Therefore, calibration curves of absorbance (at 460 and 640 nm) were constructed with DN membranes that had fully absorbed a HULK solution of a particular concentration **(Fig. S1)**. The absorbance of the samples was characterized with microplate reader (Tecan, Infinite M200 PRO). Disc samples (d ~6 mm, t ~0.5 mm, $N = 15$) were harvested from slabs (t ~0.5 mm) with a biopsy punch and each disc was placed into a well of a 96-well plate. To each well was added 300 μL HULK solution prepared in IPA (0.0018 mM, 0.0037 mM, 0.018 mM, 0.037 mM, and 0.07 mM, $N = 3$ for each "original supernatant" concentration). After 48 hr at 35 °C, each disc was removed, washed with IPA (1 mL, 3X, 10 min), and equilibrated in IPA ON at RT. The absorbance of the "final supernatant" (after the removal of disc) was recorded. Because of the transparency of all membranes equilibrated in IPA, all absorbance readings of the discs were taken while each sample was immersed in 100 μL in IPA. The HULK concentration of each disc was calculated as "moles of loaded HULK" (i.e., moles of HULK in "original supernatant" minus moles of HULK in the "final supernatant") divided by the volume of the disc (~11 μL). To determine the moles of HULK in the "final supernatant", a calibration curve was made plotting the absorbance versus concentration (0.01 mM, 0.05 mM, 0.1 mM, and 0.2 mM) of HULK IPA solutions (**Fig S2**).

Fabrication of biosensors (HULK- and GOx-containing DN membranes). In addition to the incorporation of HULK, GOx was incorporated into DN membranes to form the biosensors. The aforementioned HULK-containing DN membrane disc specimens, equilibrated in DI, were

sequentially soaked in 2.5 % (w/v) of glutaraldehyde aqueous solution (300 μL) for 1.5 hr and GOx aqueous solution ON. In between these two soakings, each disc was washed with DI (1 mL, 3 × 10 min) and equilibrated in DI for 1 hr. The resulting biosensors were stored in 5 mM NaAc solution (pH ~5) in refrigerator prior to all testing.

The GOx activity was determined using a colorimetric activity assay kit. The disc samples were placed in a 96 well-plate and were equilibrated in 5 mM NaAc solution at 37 °C prior to testing. After 10 min, the NaAc solution was removed, followed by the addition of 150 μL activity assay solution (pH ~5, at 37 ºC), which was comprised of 145 μL of 0.17 mM *o*-DDH and 1.72% (w/v) glucose (dissolved in 50 mM NaAc solution), and 5 μL 60 unit/mL POD aqueous solution. Immediately after the addition, the absorbance at 500 nm was recorded every 15 s for 5 min. The GOx enzyme activity was calculated with equation 5 ($\frac{\Delta Ab_{500nm}}{min}_{test}$: absorbance changes within one min for testing samples; $\frac{\Delta Ab_{500nm}}{min}_{blank}$: absorbance changes within one min for blank cells; ε: molar attenuation coefficient of oxidized *o*-DDH at 500 nm, which equals 7.5 $mM^{-1}•cm^{-1}$; l: light pathlength, which was measured to be ~0.5 cm; V_{assay}: volume of the assay, which was 150 μL; and V_{disc}: volume of the disc, which was calculated to be ~11 μL).

$$\frac{Units}{mL} of\ enzyme = \left(\frac{\frac{\Delta Ab_{500nm}}{min}_{test} - \frac{\Delta Ab_{500nm}}{min}_{blank}}{\varepsilon * l} \right) * \frac{V_{assay}}{V_{disc}} \quad (5)$$

Oxygen permeability of biosensors. Biosensors (d ~6 mm, t ~0.5 mm, *N* = 3 per composition) were fabricated from DN membrane containing ~0.3 mM HULK and ~100 unit/mL GOx. For each composition, three samples were immersed in 15 mL NaAc buffer solution (5 mM, pH ~5) within a 20 mL scintillation vial and were degassed by bubbling with N_2 for 1 hr. The scintillation vials were than sealed with parafilm and equilibrated at 37 °C. Each sample was quickly placed in a cell

of a 96-well plate containing 80 μL DI, which was equilibrated in open container to air overnight. The phosphorescence intensity (fluorescence intensity at excitation [460 nm], emission [800 nm], and lag time [25 μs]) changes of the sample were recorded over 1 min. As the phosphorescence intensity changing rate is directly related to oxygen permeability, the slope of phosphorescence intensity versus time was calculated and used as indicator for oxygen permeability.

Glucose sensitivity of biosensors. Biosensors (d ~6 mm, t ~0.5 mm, $N = 3$ per composition) were fabricated from each DN membrane containing ~0.3 mM HULK and ~100 unit/mL GOx. For each composition, three samples were equilibrated in 15 mL NaAc solution (5 mM) at 37 °C. Each sample was placed into one cell of a 96-wellplate and 50 μL glucose solution (0, 50, 100, 150, 200, or 300 mg/dL) was added and the discs equilibrated for precisely 5 min (at 37 ºC). The phosphorescence intensity (fluorescence intensity at excitation [460 nm], emission [800 nm], and lag time [25 μs]) were recorded over a 5 min equilibration. The normalized phosphorescence intensity (intensity at 0 min equilibrating in NaAc solution / intensity at 5 min equilibrating in given glucose solution) was calculated for each glucose concentration to value the sensitivity. A given sample was sequentially equilibrated with glucose solutions of increasing concentration, washing 3X with 5 mM NaAc solution with 5 min in between.

Cytocompatibility of biosensors. Biosensor discs (d ~6 mm x t ~0.5 mm, $N = 3$, from different hydrogel sheets) were similarly prepared. After loading with 0.3 mM of HULK, discs were sterilized by soaking in 70% (v/v) ethanol (30 min × 3) and recovered in sterile PBS (30 min × 3). After sterilization, ~100 unit/mL GOx was incorporated by sequentially soaking discs in glutaraldehyde and GOx solutions. Mouse fibroblast cells (NIH/3T3) (ATCC) were cultured under normal media conditions consisting of Dulbecco's Modified Eagle's Medium (DMEM) with 10 % FBS and 1% penicillin/streptomycin (100 U/100 μg/mL). After every 2-3 days, culture media was

exchanged for fresh media. Cells were passaged with 0.5% trypsin-EDTA upon reaching confluency of ~70% and seeded at ~2500 cells/cm^2. For indirect cellular viability assay, NIH/3T3 cells were cultured in a 24 well plate at 10,000 cells per wells. Discs were placed with a transwell insert, which were then placed within the 24 well plate, with cells without transwell inserts acting as control (N = 3). After 24 hr at 37 °C, cellular viability was determined using alamarBlue™ according to manufactured protocol. For cellular morphology studies, NIH/3T3 cells were seeded directly on to hydrogels of different compositions for 24 hr at 37 °C, with cells cultured in a 96 well plate acting as control. For actin staining, cells were, fixed with 2.5% glutaraldehyde and permeabilized with 0.1% TritonX-100. Phalloidin stain was then added (per manufacturer's protocol) and samples were incubated for 20 min at 37 °C. The stain was removed, washed with 1X PBS (x 3). Cells were then treated with Hoechst 33258 according to manufacturer's protocol and incubated for 5 min at RT. Samples were then washed with 1X PBS (x 3) followed by imaging using a fluorescent inverted microscope (ZEISS Axio Vert.A1).

Statistical Analysis: All data included are reported as means ± standard deviations (i.e. error bar). All the statistical analysis comparison was done in GraphPad Prism with 1-way or 2-way ANOVA, when the statistical significance was assumed with a p-value $\leqslant 0.05$.

Results and Discussion

Membrane fabrication. DN hydrogel membranes were fabricated to achieve an even distribution of the silicone phase as microdomains dispersed throughout the hydrogel matrices **(Scheme 2a**, **Table 1)**. Using ultrasonication, the 1st network precursor emulsion was formed, comprised of silicone microdroplets dispersing within the aqueous phase. The emulsions exhibited no visible phase separation, even after 30 days (**Fig. S3**). As the silicone phase concentration increased, the

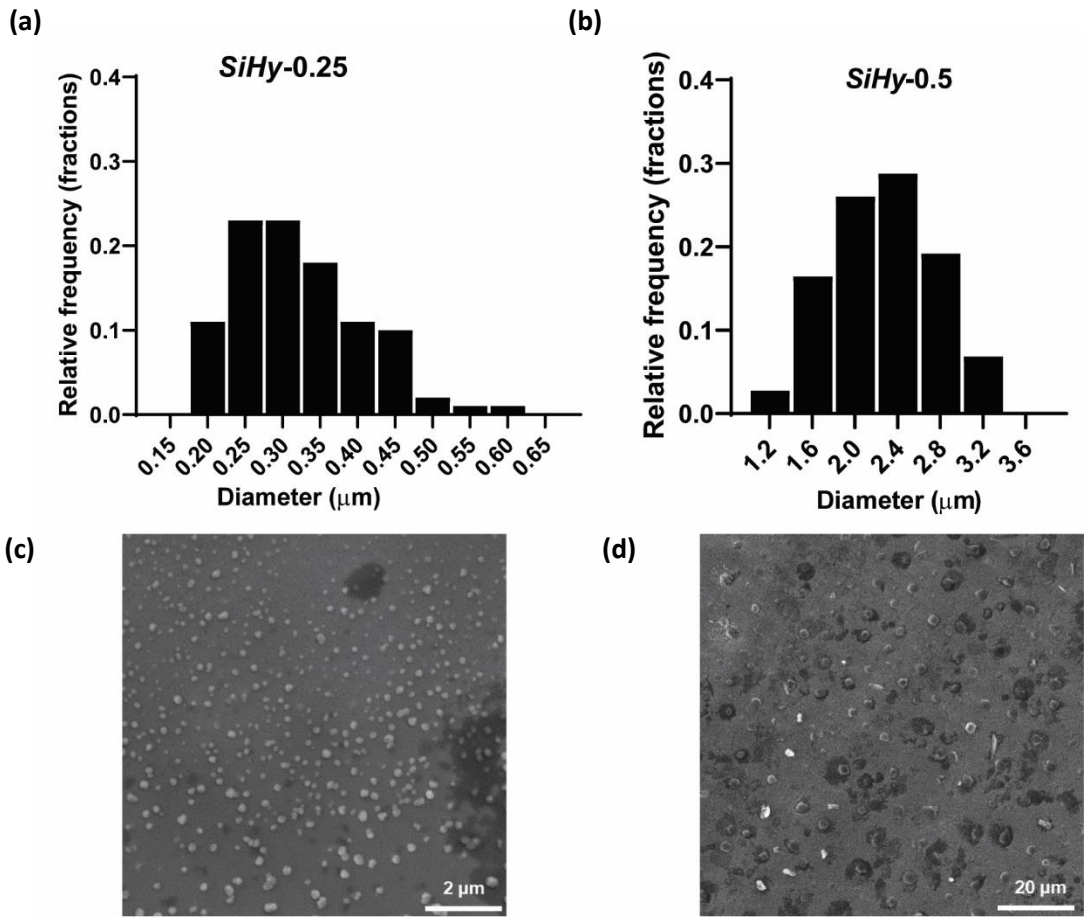

Figure 1. Size of silicone-based microdroplets in the 1st network precursor emulsions and representative SEM images of corresponding membranes for **(a, c)** *SiHy*-0.25 and **(b, d)** *SiHy*-0.5.

average diameter of microdroplets increased in the precursor emulsion: 0.32 ± 0.08 μm [*SiHy-0.25*] and 2.24 ± 0.5 μm [*SiHy*-0.50] (**Fig. 1**).

A variety of analyses were performed to confirm the presence of crosslinked silicone microdomains within *SiHy*-0.25 and *SiHy*-0.5. Following sequential UV curing, the resulting DN membranes were sequentially equilibrated in 100% IPA and DI water (**Fig. 2a**). Devoid of silicone microdomains, *SiHy*-0 was transparent in both water and IPA. Because of the incompatibility of the silicone chains with water, the opacity of *SiHy*-0.5 more pronounced than that of *SiHy*-0.25. These membranes became transparent when equilibrated in IPA due to the improved solvent

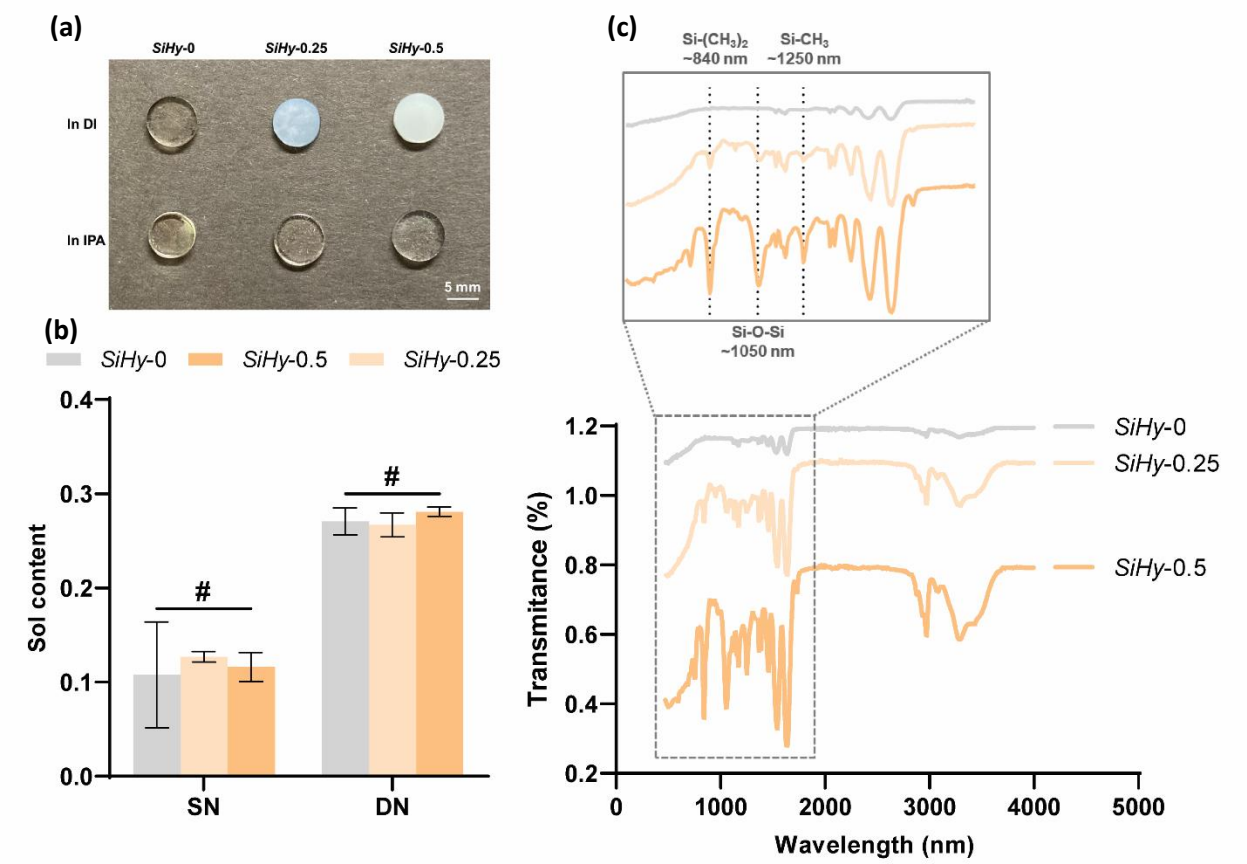

Figure 2. (a) Representative photo image of *SiHy*-x (x = 0, 0.25, or 0.5) discs immersed in DI or IPA. **(b)** Sol content of both SN and DN membranes. **(c)** Representative ATR-FTIR curves of *SiHy*-x (x = 0, 0.25 and 0.5). Peaks associated with silicone microparticles labeled: Si-CH_3 (~1250 nm), Si-O-Si (~1050 nm) and Si$(CH_3)_2$ (~840 nm). (#: $p > 0.05$, no significant difference).

compatibility with the microdomains, but the opacity was recovered upon returning to water. Additionally, following soaking in IPA, the sol content values of SN membranes and their corresponding DN membranes was not impacted by the presence of silicone microdomains **(Fig. 2b)**. This indicates the UV curing process was not compromised. Lastly, ATR-FTIR confirmed the presence of silicone in *SiHy*-0.25 and *SiHy*-0.5 based on the following peaks: Si-$(CH_3)_2$ (~840 nm), Si-O-Si (~1050 nm) and Si-(CH_3) (~1250 nm) **(Fig. 2c)**.

DN membranes were exposed to Nile red to stain hydrophobic silicone microdomains and to view distribution via CLSM **(Fig. 3)**. While *SiHy*-0 expectedly showed no stained component,

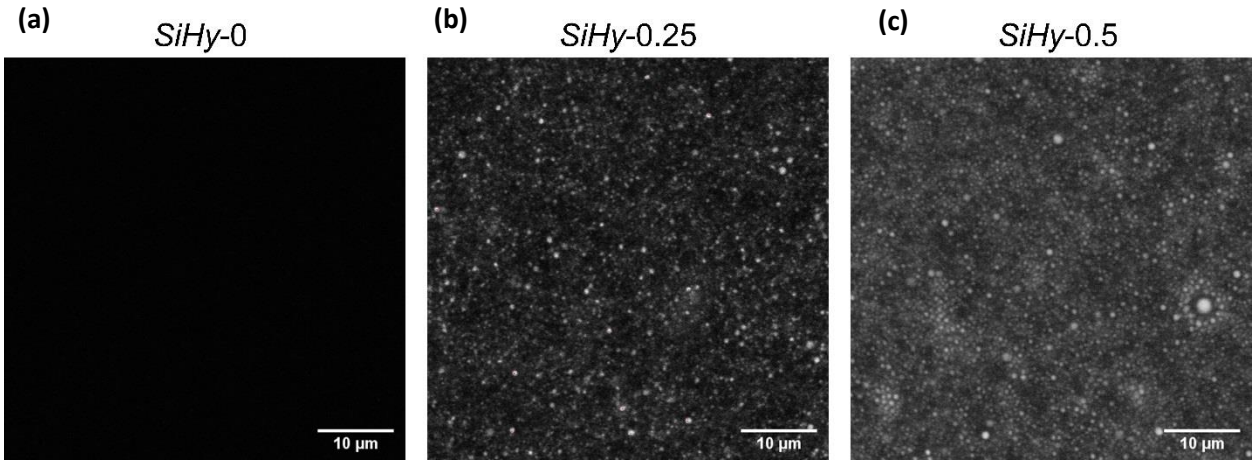

Figure 3. Representative CLSM images (in black and white) of **(a)** *SiHy*-0, **(b)** *SiHy*-0.25, and **(c)** *SiHy*-0.5. (Scale bar = 10 µm)

SiHy-0.25 and *SiHy*-0.5 exhibited the clear presence of discrete microdomains. The microdomains of *SiHy*-0.5 were larger than that of *SiHy*-0.25, consistent with microdroplet sizes observed in emulsions (**Fig. 1**). For *SiHy*-0.5, some apparent aggregation of the silicone microdomains was observed.

SEM and EDS were used to characterize the DN membrane cross-sections **(Fig. 4, Fig. S4)**. Silicone elements stemming from the microparticles were detected for *SiHy*-0.25 and *SiHy*-0.5, but expectedly absent in *SiHy*-0. Interestingly, a rough morphology indicative of subtle phase separation was observed exclusively for *SiHy*-0.25.

Membrane properties. A specific VPTT profile of T_{onset} ~36.5 °C was targeted for these DN membranes. This was intended to recapitulate that of our previously reported thermoresponsive membranes which exhibited exceptional biocompatibility associated with limiting cellular adhesion via cyclical deswelling/reswelling corresponding to temperature fluctuations in the subcutaneous tissue.[56] This was achieved by addition of 5 wt% of a hydrophilic comonomer (AAm) into the 2nd networks of DN membranes **(Table 1)**. The VPTT profiles did not significantly vary

for DN membranes. Thus, while hydrophobic comonomers reduce the VPTT of NIPAAm-based networks,[75-76] silicone microparticles conveniently did not due to their discrete nature.

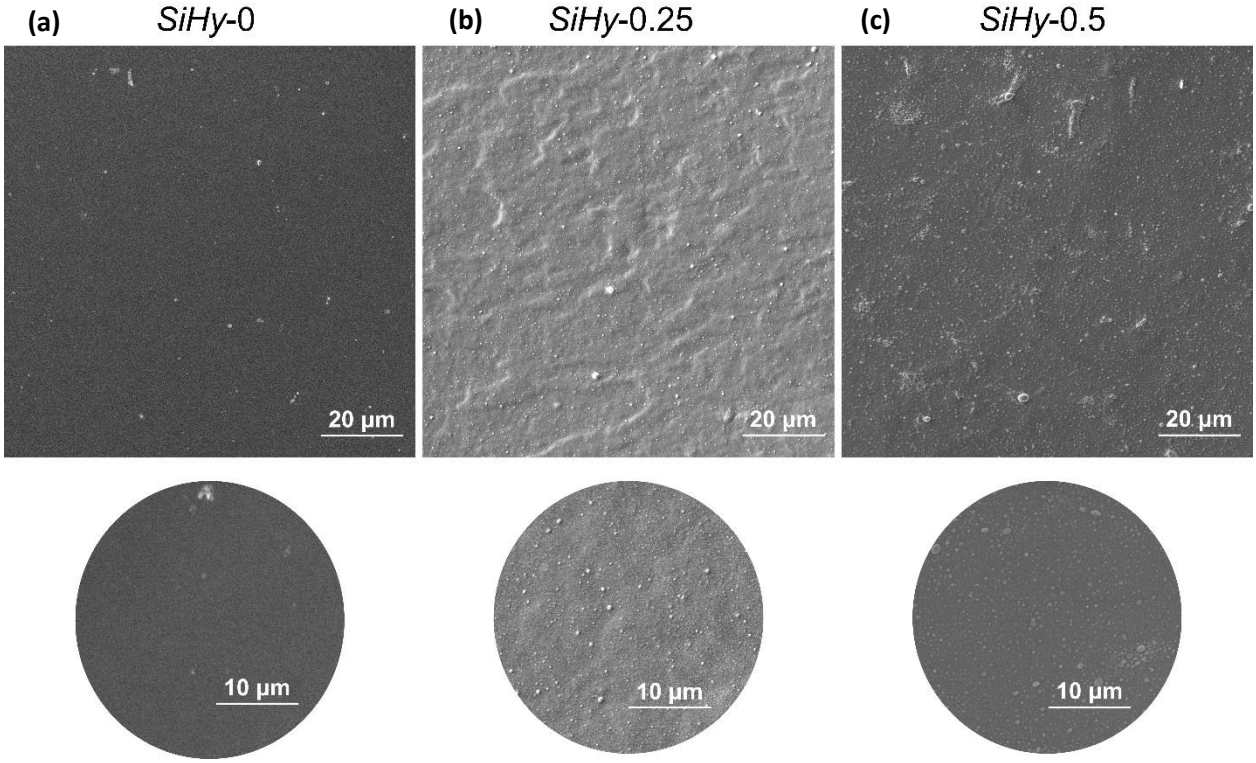

Figure 4. Representative SEM images of cross-sections for: **(a)** *SiHy*-0, **(b)** *SiHy*-0.25, and **(c)** *SiHy*-0.5. (Top row scale bars = 20 µm; bottom row scale bars = 10 µm.)

The surface hydrophilicity decreased with increasing hydrophobic silicone microparticle content **(Fig. 5a)**. As the droplet just contacted with the slab (0 min), contact angles > 90 ° were observed for *SiHy*-0 (~94 °), *SiHy*-0.25 (~101 °), and *SiHy*-0.5 (~108 °). After 1 min, the contact angles decreased to below 90 ° (*SiHy*-0: ~61 °, *SiHy*-0.25: ~78 °, and *SiHy*-0.5: ~85 °), but this may be due to absorption of the water droplet. Thus, bulk hydrophilicity was also assessed. The water contents of all DN membranes were similar (**Table 1**). However, H-index measurements revealed the expected decrease in bulk hydrophilicity (i.e., increase H-index) with increasing silicone microparticle content **(Fig. 5b)**. While differences in bulk hydrophilicity may alter aqueous

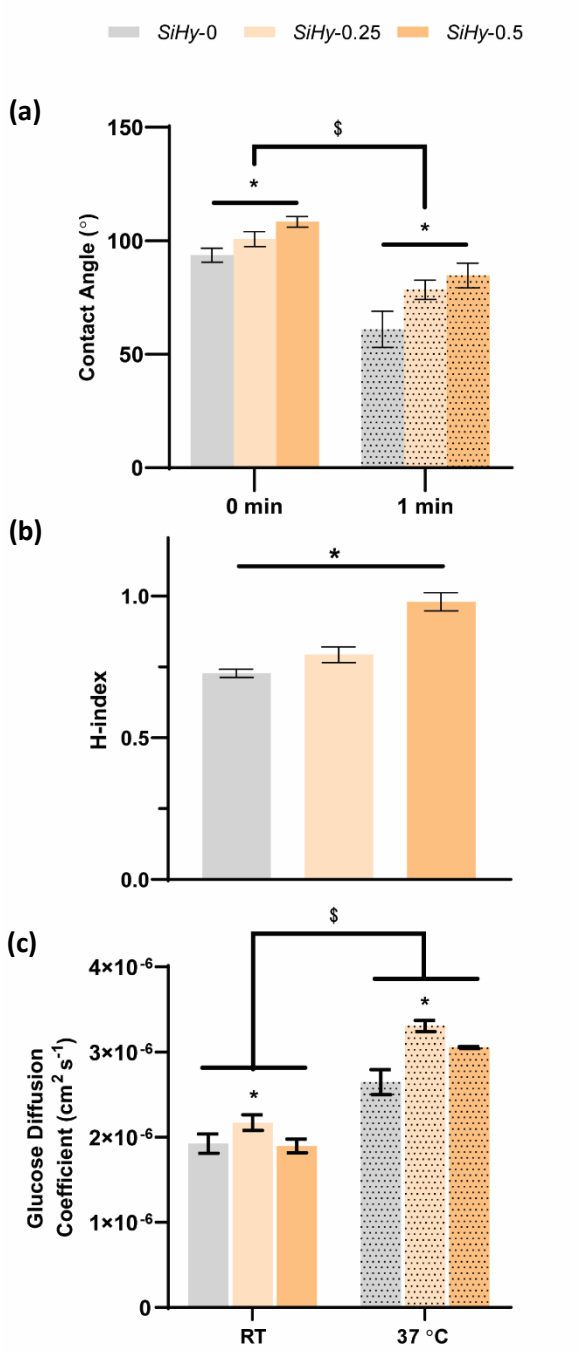

Figure 5. For *SiHy*-x (x = 0, 0.25 or 0.5): **(a)** Contact angle of water droplet at t = 0 (0 min) and t = 1 min. **(b)** H-index values. **(c)** Glucose diffusion coefficients. (*: $p < 0.05$, significantly different versus other membranes at the same temperature; $: $p < 0.05$, *SiHy*-0, *SiHy*-0.25, or *SiHy*-0.5 significantly different versus itself at different temperature).

diffusion processes, glucose diffusion coefficients were not found to be substantially different **(Fig. 5c)**. Due to their thermosensitivity, glucose diffusion tests were conducted at both RT (22 °C) (i.e.,

fully swollen state) and 37 °C (i.e., onset of deswollen state, respectively). For all DN membranes, the slight increase in diffusion at the higher temperature was attributed to a greater Brownian motion. While the most hydrophobic, *SiHy*-0.5 showed statistically similar glucose diffusion coefficient to *SiHy*-0 at both RT and 37 °C. Interestingly, a statistically-significant increase in glucose diffusion coefficient was observed of *SiHy*-0.25 at both temperatures. We speculate this may be due to the apparent phase separation of *SiHy*-0.25 (**Fig. 4**). Important to their utility to form glucose biosensors, all DN membranes displayed glucose diffusion coefficients greater than that of the subcutaneous tissue (~2×10^{-6} cm^2 s^{-1}).[77]

The mechanical properties of the DN membranes were directly impacted by the presence of silicone microparticles (**Fig. 6**). As microparticle concentration increased, modulus decreased while %strain increased; these changes are attributed to the elastomeric nature of silicone microparticles. Owing to the enhanced elasticity and perhaps strain-induced strengthening, *SiHy*-0.5 exhibited greater strength. The toughness of *SiHy*-0.5 also exceeded that of *SiHy*-0 and *SiHy*-0.25. It is notable to compare the mechanical properties of these DN membranes to that of poly(ethylene glycol) diacrylate (PEG-DA) hydrogels which are often explored for implantable materials, including those based on PEG-DA (3.4 kDa, 10 wt%) and likewise evaluated in compression tests to yield: modulus (~0.22 MPa), strength (0.13 MPa), and toughness (0.0148 MJ/m^3).[56] In this regard, *SiHy*-0.25 and *SiHy*-0.50 exhibited robust mechanical properties.

Fabrication of biosensors. Biosensors (i.e., membranes containing HULK and GOx) (discs; d ~6 mm, t ~0.5 mm) were prepared per **Scheme 2b**. The cytocompatibility was confirmed via indirect contact method, where hydrogel discs were places in a transwell insert and the metabolic activity of seeded cells were monitored. No significance change in metabolic activity was observed over a course of 24 hours (**Fig. S5**). To evaluate the effect of silicone microdomains on cell adhesion,

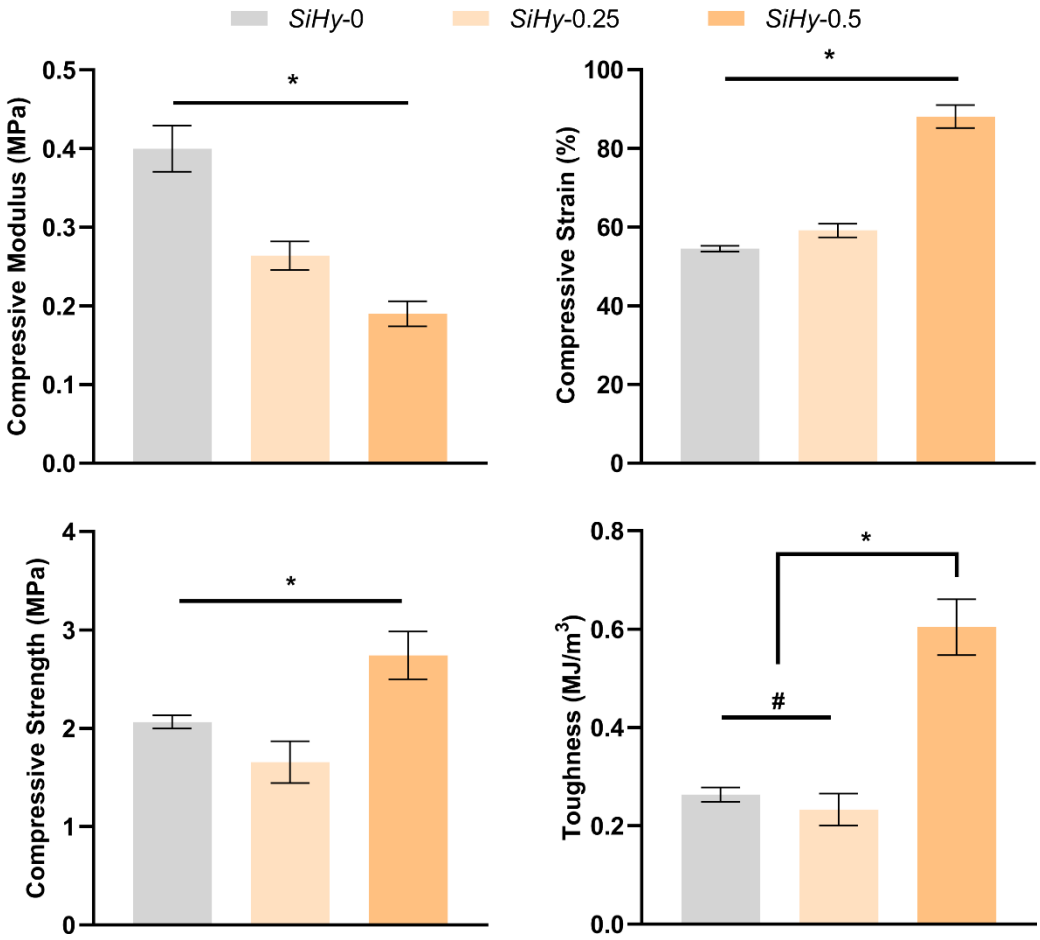

Figure 6. Mechanical properties of *SiHy*-x (x = 0, 0.25 or 0.5) (*: $p < 0.05$, significantly different; #: $p > 0.05$, no significant difference).

cells were imaged after seeded on the hydrogel surface. On positive control (TCPS), attached cells demonstrated normal morphology. As expected, no significant cell spreading was observed on DN membranes, supporting previous observation.[61] Interestingly, incorporating of silicone microdomains to DN membranes did not have any appreciable effect on cells spreading, including on *SiHy*-0.25 and *SiHy*-0.5, despite their greater hydrophobicity. This was unexpected as prior work indicated that an increase in hydrophobicity improve protein adsorption on the surface, which resulted enhanced cells adhesion and spreading.[78] However, while membrane bulk hydrophobicity increased with silicone microparticle content, surface contact angle analysis showed no

discernable change (**Fig. 5**). While the latter was attributed to potential diffusion of the water droplet, it is also possible that hydrophobic silicone microdomains may not be appreciably at the surface of the membranes. A lack of cellular adhesion could also be attributed to the similarly high water contents (>87%) of all membranes (**Table 1**).

Similar HULK concentration (~0.3 mM) and the GOx concentration (~100 unit/mL) were determined among *SiHy*-0, *SiHy*-0.25 and *SiHy*-0.5 samples **(Fig. 7a** and **b)**. The oxygen permeability was indirectly accessed by measuring the phosphorescence intensity changes within the first minute as the biosensors were exposed to aqueous environment containing saturated oxygen **(Fig. 7c)**. Versus *SiHy*-0, the silicone microdomain-containing biosensors *SiHy*-0.25 and *SiHy*-0.5 both exhibited a faster rate change, indicative of improved oxygen permeability. Interestingly, the *SiHy*-0.25 biosensor displayed greater oxygen permeability versus the *SiHy*-0.5 biosensor. This trend paralleled the increase in glucose diffusion coefficient (**Fig. 5c**) and is likewise attributed to the apparent phase separation of *SiHy*-0.25. Finally, glucose sensing was characterized with phosphorescence intensity changes upon exposure to biosensors increasing glucose concentrations (0, 50, 100, 150, 200 and 300 mg/dL) **(Fig. 7d)**. In our prior work,[62] the *SiHy*-0 biosensor (t ~1.2 mm) exhibited glucose sensitivity limited to concentrations of 50 to 100 mg/dL. Herein, by reducing *SiHy*-0 biosensor thickness (t ~0.5 mm), glucose sensitivity was achieved from 100 to 150 mg/dL. Despite having highest concentration of silicone microdomain, the sensitivity of a *SiHy*-0.5 biosensor paralleled that of *SiHy*-0 biosensor. However, the *SiHy*-0.25 biosensor notably showed sensitivity in the range of 100 to 300 mg/dL. A lack of sensitivity at lower concentration (50 - 100 mg/dL) noted for all membranes was attributed to decreased thickness, allowing for fast oxygen permeability and concomitant over consumption at low glucose conditions.

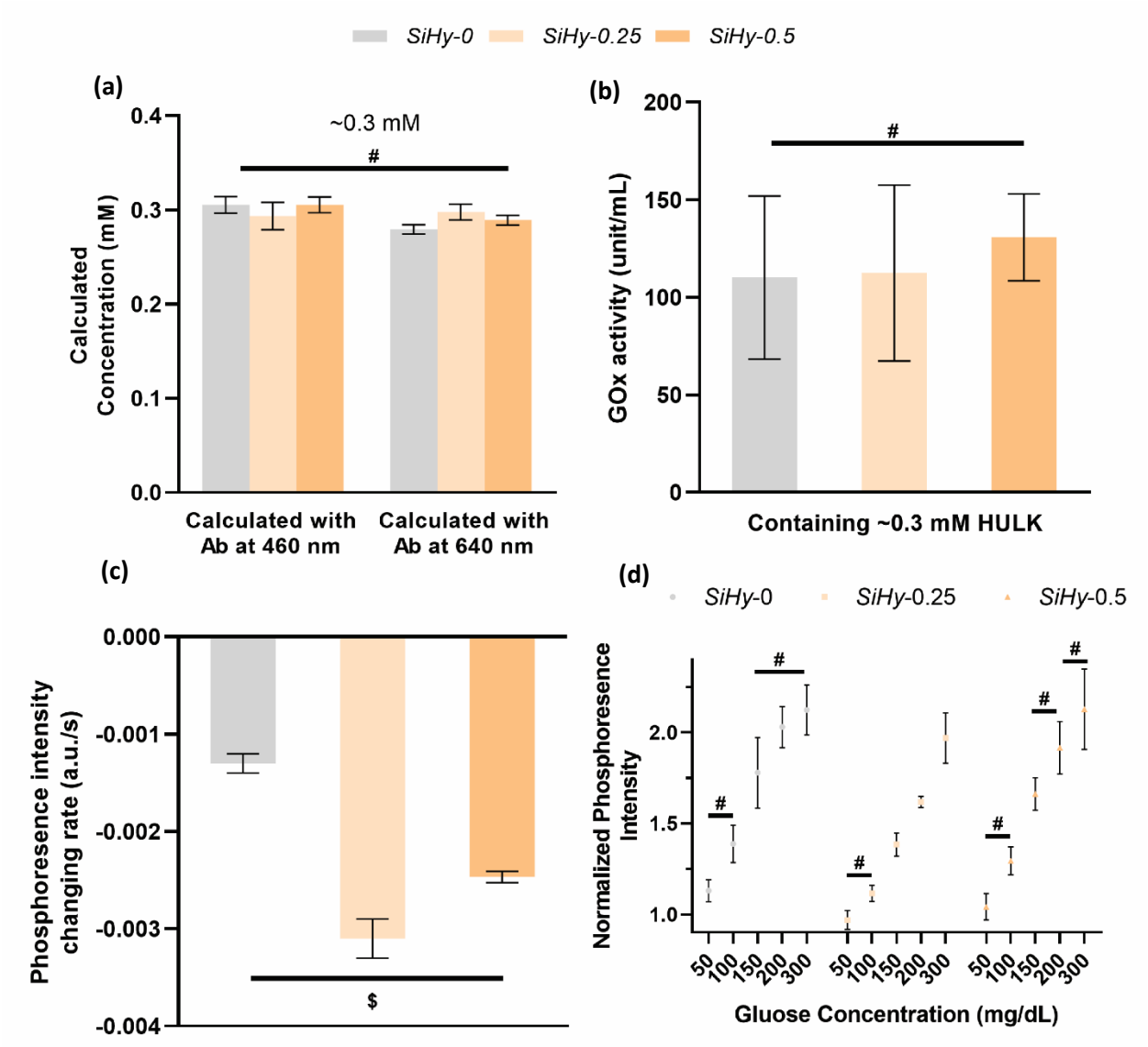

Figure 7. For biosensors prepared from HULK and GOx-containing *SiHy*-0, 0.25 or 0.5: **(a)** Calculated concentration of HULK. **(b)** GOx activity. **(c)** Phosphorescence intensity changing rate within the first minute of exposure to an oxygen-saturated aqueous solution. (#: $p > 0.05$, no significant difference; $: $p < 0.05$, significantly different)

Conclusion

Towards creating an injectable subcutaneous glucose biosensor, a thermoresponsive DN membrane was customized to house the metalloporphyrin $PdPh_4(SO_3Na)_4TBP_3$ (i.e., "HULK") and GOx. For this glucose sensing assay, the phosphorescence intensity or lifetime of HULK can

be related to glucose levels as oxygen is consumed via glucose oxidation as catalyzed by GOx. Because of this oxygen sensitivity, the membrane must be adequately permeable to oxygen. A thermoresponsive DN membrane design, previously shown to limit the FBR reaction via body temperature fluctuation-driven cyclical swelling/deswelling, was thus strategically tailored to house HULK and GOx as well as to enhance oxygen permeability. To improve oxygen permeability, silicone microparticles were incorporated into the DN membranes at two concentrations, resulting in *SiHy*-0.25 and *SiHy*-0.5 compositions. Silicone emulsions were ~~used~~ effectively introduced during formation of the P[NIPAAm-*co*-APTAC] 1st network, and DN membranes formed by subsequent curing of the P[NIPAAm-*co*-AAm] 2nd network. HULK and GOx were immobilized within the membranes via electrostatic and hydrophobic interactions, respectively. The presence of the silicone microparticles within the membranes was confirmed with solubility testing, ATR-FTIR, and SEM/EDS. The targeted VPTT profile for these membranes was maintained, attributed to the discrete nature of the silicone microparticles. As expected, increasing levels of hydrophobic silicone microparticles led to reduced surface and bulk hydrophilicity of membranes. However, the water content of the membranes remained similarly high. Owing to the elastomeric nature of crosslinked silicone chains, membrane modulus decreased while %strain increased with increasing microparticle content. Still, *SiHy*-0.25 and *SiHy*-0.5 were more mechanically robust versus conventional PEG-DA hydrogels. For both membranes, glucose diffusion coefficients were favorably greater than that of the control membrane (*SiHy-0*) and subcutaneous tissue. Both membranes displayed superior oxygen permeability versus *SiHy-0*. However, oxygen permeability as well as glucose permeability was the greatest for *SiHy-0.25*, and was attributed to its apparent phase separation of ~~*SiHy*-0.25~~ as observed ~~in~~ by SEM ~~images~~. Based on phosphoresce intensity measurements, *SiHy*-0.25

biosensors (i.e., containing HULK and GOx) also showed the broadest glucose sensitivity range (100 - 300 mg/dL) versus *SiHy*-0 and *SiHy*-0.5 biosensors (100-150 mg/dL). Thus, the *SiHy*-0.25 biosensor represents a promising subcutaneous glucose biosensor and warrants future *in vivo* assessment.

Supporting Information

Additional experimental results such as calibration curves, images of precursor emulsions, SEM images, EDS data, cytocompatibility images and data, and data corresponding to figures.

Author contributions

The manuscript was written through contributions of all authors. All authors have given approval to the final version of the manuscript.

Conflicts of interest

There are no conflicts to declare.

Acknowledgements

Funding from the National Science Foundation (NSF) Engineering Research Center (ERC) for Precise Advance Technologies and Health Systems (PATHS-UP) (Award No. 1648451) is gratefully acknowledged. The use of the Texas A&M Microscopy and Imaging Center is acknowledged.

References

1. Organization, W. H. *Global report on diabetes: executive summary*; World Health Organization: 2016.
2. Organization, W. H., Global report on diabetes. 2016.
3. Roglic, G. e., WHO Global report on diabetes: A summary. *Int. J. Non-Commun. Dis.* **2016,** *1* (1), 3.
4. Prevention, C. f. D. C. *National diabetes statistics report, 2020*; Centers for Disease Control Prevention, US Department of Health Human Services: Atlanta, GA, 2020.
5. Manavalan, D.; Wen, C.; Young, C. F.; Farhangi, V., Diabetes technology: the present and the future. *Prim. Care Rep.* **2021,** *27* (6).
6. Real-world safety of an implantable continuous glucose sensor over multiple cycles of use: A post-market registry study. **2020,** *22* (1), 48-52.
7. Sheng, T.; Offringa, R.; Kerr, D.; Clements, M.; Fischer, J.; Parks, L.; Greenfield, M., Diabetes healthcare professionals use multiple continuous glucose monitoring data indicators to assess glucose management. *J. Diabetes Sci. Technol.* **2019,** *14* (2), 271-276.
8. Sanchez, P.; Ghosh-Dastidar, S.; Tweden, K. S.; Kaufman, F. R., Real-world data from the first U.S. commercial users of an implantable continuous glucose sensor. *Diabetes Technol. Ther.* **2019,** *21* (12), 677-681.
9. Battelino, T.; Danne, T.; Bergenstal, R. M.; Amiel, S. A.; Beck, R.; Biester, T.; Bosi, E.; Buckingham, B. A.; Cefalu, W. T.; Close, K. L.; Cobelli, C.; Dassau, E.; DeVries, J. H.; Donaghue, K. C.; Dovc, K.; Doyle, F. J.; Garg, S.; Grunberger, G.; Heller, S.; Heinemann, L.; Hirsch, I. B.; Hovorka, R.; Jia, W.; Kordonouri, O.; Kovatchev, B.; Kowalski, A.; Laffel, L.; Levine, B.; Mayorov, A.; Mathieu, C.; Murphy, H. R.; Nimri, R.; Nørgaard, K.; Parkin, C. G.; Renard, E.; Rodbard, D.; Saboo, B.; Schatz, D.; Stoner, K.; Urakami, T.; Weinzimer, S. A.; Phillip, M., Clinical targets for continuous glucose monitoring data interpretation: recommendations from the international consensus on time in range. *Diabetes Care* **2019,** *42* (8), 1593.
10. Ajjan, R.; Slattery, D.; Wright, E., Continuous glucose monitoring: A brief review for primary care practitioners. *Adv Ther* **2019,** *36* (3), 579-596.
11. Engler, R.; Routh, T. L.; Lucisano, J. Y., Adoption barriers for continuous glucose monitoring and their potential reduction with a fully implanted system: results from patient preference surveys. *Clin. Diabetes* **2018,** *36* (1), 50-58.
12. Welsh, J. B.; Thomas, R., Continuous glucose monitoring: an emerging standard of care. *Am J Manag Care* **2019,** *25* (4 Spec No.), Sp116-sp119.
13. Jernelv, I. L.; Milenko, K.; Fuglerud, S. S.; Hjelme, D. R.; Ellingsen, R.; Aksnes, A., A review of optical methods for continuous glucose monitoring. *Appl. Spectrosc. Rev.* **2019,** *54* (7), 543-572.
14. Ward, W. K., A review of the foreign-body response to subcutaneously-implanted devices: the role of macrophages and cytokines in biofouling and fibrosis. *J. Diabetes Sci. Technol.* **2008,** *2* (5), 768-777.
15. Tanenbaum, M. L.; Hanes, S. J.; Miller, K. M.; Naranjo, D.; Bensen, R.; Hood, K. K., Diabetes device use in adults with type 1 diabetes: barriers to uptake and potential intervention targets. *Diabetes Care* **2017,** *40* (2), 181-187.
16. Senseonics Long-term CGM System / Eversense Continuous Glucose Monitoring. https://www.eversensediabetes.com/eversense-cgm-system (accessed January 1).

17. Christiansen, M. P.; Klaff, L. J.; Brazg, R.; Chang, A. R.; Levy, C. J.; Lam, D.; Denham, D. S.; Atiee, G.; Bode, B. W.; Walters, S. J., A prospective multicenter evaluation of the accuracy of a novel implanted continuous glucose sensor: PRECISE II. *Diabetes Technol. Ther.* **2018,** *20* (3), 197-206.
18. administration, U. S. f. a. d., Eversense E3 continuous glucose monitoring system - P160048/S016. u.s. food and drug administration: 2022; Vol. 2022.
19. McNichols, R. J.; Coté, G. L., Optical glucose sensing in biological fluids: an overview. *J. Biomed. Opt.* **2000,** *5* (1), 5-16.
20. Oliver, N. S.; Toumazou, C.; Cass, A. E.; Johnston, D. G., Glucose sensors: a review of current and emerging technology. *Diabet. Med.* **2009,** *26* (3), 197-210.
21. Yu, Z.; Jiang, N.; Kazarian, S. G.; Tasoglu, S.; Yetisen, A. K., Optical sensors for continuous glucose monitoring. *Prog. Biomed. Eng.* **2021,** *3* (2), 022004.
22. Bobrowski, T.; Schuhmann, W., Long-term implantable glucose biosensors. *Curr. Opin. Electrochem.* **2018,** *10*, 112-119.
23. Gerritsen, M.; Jansen, J. A.; Kros, A.; Vriezema, D. M.; Sommerdijk, N. A. J. M.; Nolte, R. J. M.; Lutterman, J. A.; Van Hövell, S. W. F. M.; Van der Gaag, A., Influence of inflammatory cells and serum on the performance of implantable glucose sensors. **2001,** *54* (1), 69-75.
24. Onuki, Y.; Bhardwaj, U.; Papadimitrakopoulos, F.; Burgess, D. J., A review of the biocompatibility of implantable devices: current challenges to overcome foreign body response. *J. Diabetes Sci. Technol.* **2008,** *2* (6), 1003-1015.
25. Xu, J.; Lee, H., Anti-biofouling strategies for long-term continuous use of implantable biosensors. *Chemosensors* **2020,** *8* (3), 66.
26. Scholten, K.; Meng, E., A review of implantable biosensors for closed-loop glucose control and other drug delivery applications. *Int. J. Pharm.* **2018,** *544* (2), 319-334.
27. Nichols, S. P.; Koh, A.; Storm, W. L.; Shin, J. H.; Schoenfisch, M. H., Biocompatible materials for continuous glucose monitoring devices. *Chem. Rev.* **2013,** *113* (4), 2528-2549.
28. Dautta, M.; Alshetaiwi, M.; Escobar, J.; Tseng, P., Passive and wireless, implantable glucose sensing with phenylboronic acid hydrogel-interlayer RF resonators. *Biosens. Bioelectron.* **2020,** *151*, 112004.
29. Yetisen, A. K.; Jiang, N.; Fallahi, A.; Montelongo, Y.; Ruiz-Esparza, G. U.; Tamayol, A.; Zhang, Y. S.; Mahmood, I.; Yang, S.-A.; Kim, K. S.; Butt, H.; Khademhosseini, A.; Yun, S.-H., Glucose-sensitive hydrogel optical fibers functionalized with phenylboronic acid. *Advanced Materials* **2017,** *29* (15), 1606380.
30. Bornhoeft, L. R.; Biswas, A.; McShane, M. J., Composite hydrogels with engineered microdomains for optical glucose sensing at low oxygen conditions. *Biosensors* **2017,** *7* (1), 8.
31. Li, D.-J.; Ohsaki, K.; Ii, K.; Cui, P.-C.; Ye, Q.; Baba, K.; Wang, Q.-C.; Tenshin, S.; Takano-Yamamoto, T., Thickness of fibrous capsule after implantation of hydroxyapatite in subcutaneous tissue in rats. *J. Biomed. Mater. Res.* **1999,** *45* (4), 322-326.
32. Ward, W. K.; Slobodzian, E. P.; Tiekotter, K. L.; Wood, M. D., The effect of microgeometry, implant thickness and polyurethane chemistry on the foreign body response to subcutaneous implants. *Biomaterials* **2002,** *23* (21), 4185-4192.
33. Irwin, E. F.; Saha, K.; Rosenbluth, M.; Gamble, L. J.; Castner, D. G.; Healy, K. E., Modulus-dependent macrophage adhesion and behavior. *J. Biomater. Sci. Polym. Ed.* **2008,** *19* (10), 1363-1382.

34. Klueh, U.; Kaur, M.; Montrose, D. C.; Kreutzer, D. L., Inflammation and glucose sensors: use of dexamethasone to extend glucose sensor function and life span in vivo. *J. Diabetes. Sci. Technol.* **2007,** *1* (4), 496-504.
35. Vallejo-Heligon, S. G.; Brown, N. L.; Reichert, W. M.; Klitzman, B., Porous, Dexamethasone-loaded polyurethane coatings extend performance window of implantable glucose sensors in vivo. *Acta Biomater.* **2016,** *30*, 106-115.
36. Jung, S.-K.; Wilson, G. S., Polymeric mercaptosilane-modified platinum electrodes for elimination of interferants in glucose biosensors. *Anal. Chem.* **1996,** *68* (4), 591-596.
37. Hetrick, E. M.; Schoenfisch, M. H., Reducing implant-related infections: active release strategies. *Chem. Soc. Rev.* **2006,** *35* (9), 780-789.
38. Yu, B.; Wang, C.; Ju, Y. M.; West, L.; Harmon, J.; Moussy, Y.; Moussy, F., Use of hydrogel coating to improve the performance of implanted glucose sensors. *Biosens. Bioelectron.* **2008,** *23* (8), 1278-1284.
39. Bae, J.; Park, J.; Kim, S.; Cho, H.; Kim, H. J.; Park, S.; Shin, D.-S., Tailored hydrogels for biosensor applications. *J. Ind. Eng. Chem.* **2020,** *89*, 1-12.
40. Quinn, C. A. P.; Connor, R. E.; Heller, A., Biocompatible, glucose-permeable hydrogel for in situ coating of implantable biosensors. *Biomaterials* **1997,** *18* (24), 1665-1670.
41. Trzebinski , J.; Moniz, A. R.-B.; Sharma, S.; Burugapalli, K.; Moussy, F.; Cass, A. E. G., Hydrogel membrane improves natch-to-batch reproducibility of an enzymatic glucose biosensor. *Electroanalysis* **2011,** *23* (12), 2789-2795.
42. Locke, A. K.; Means, A. K.; Dong, P.; Nichols, T. J.; Coté, G. L.; Grunlan, M. A., A Layer-by-Layer approach to retain a fluorescent glucose sensing assay within the cavity of a hydrogel membrane. *ACS Applied Bio Materials* **2018,** *1* (5), 1319-1327.
43. Collier, B.; Long, R.; McShane, M. In *Dual-probe luminescence lifetime measurements for the oxygen compensation in enzymatic biosensors*, SENSORS, 2009 IEEE, 25-28 Oct. 2009; 2009; pp 703-706.
44. Collier, B. B.; McShane, M. J., Dynamic windowing algorithm for the fast and accurate determination of luminescence lifetimes. *Anal. Chem.* **2012,** *84* (11), 4725-4731.
45. Collier, B. B.; McShane, M. J., Time-resolved measurements of luminescence. *Journal of Luminescence* **2013,** *144*, 180-190.
46. Biswas, A.; Bornhoeft, L. R.; Banerjee, S.; You, Y.-H.; McShane, M. J., Composite Hydrogels Containing Bioactive Microreactors for Optical Enzymatic Lactate Sensing. *ACS Sensors* **2017,** *2* (11), 1584-1588.
47. You, Y.-H.; Biswas, A.; Nagaraja, A. T.; Hwang, J.-H.; Coté, G. L.; McShane, M. J., Multidomain-based responsive materials with dual-mode optical readouts. *ACS Appl. Mater. Interfaces* **2019,** *11* (15), 14286-14295.
48. Falohun, T.; McShane, M. J., An optical urate biosensor based on urate oxidase and long-lifetime metalloporphyrins. *Sensors* **2020,** *20* (4), 959.
49. Na, R.; Stender, I.-M.; Henriksen, M.; Wulf, H. C., Autofluorescence of human skin is age-related after correction for skin pigmentation and redness. *Journal of investigative dermatology* **2001,** *116* (4), 536-540.
50. Kollias, N.; Zonios, G.; Stamatas, G. N., Fluorescence spectroscopy of skin. *Vibrational Spectroscopy* **2002,** *28* (1), 17-23.
51. Colvin, L.; Dong, P.; Means, A. K.; Grunlan, M.; Coté, G. In *Assessment of wavelengths with skin tones for an implantable FRET-based glucose biosensor*, SPIE BiOS, SPIE: 2019; p 108850Y.

52. Collier, B. B.; McShane, M. J., Dynamic Windowing Algorithm for the Fast and Accurate Determination of Luminescence Lifetimes. *Anal. Chem.* **2012,** *84* (11), 4725-4731.
53. Collier, B. B.; McShane, M. J., Temperature Compensation of Oxygen Sensing Films Utilizing a Dynamic Dual Lifetime Calculation Technique. *IEEE Sensors Journal* **2014,** *14* (8), 2755-2764.
54. Ngo, B. K. D.; Grunlan, M. A., Protein resistant polymeric biomaterials. Lett., A. M., Ed. ACS Publications: 2017.
55. Jesmer, A. H.; Wylie, R. G., Controlling experimental parameters to improve characterization of biomaterial fouling. *Front. Chem.* **2020,** *8*, 604236-604236.
56. Means, A. K.; Dong, P.; Clubb, F. J.; Friedemann, M. C.; Colvin, L. E.; Shrode, C. A.; Coté, G. L.; Grunlan, M. A., A self-cleaning, mechanically robust membrane for minimizing the foreign body reaction: towards extending the lifetime of sub-Q glucose biosensors. *Journal of Materials Science: Materials in Medicine* **2019,** *30* (7), 79.
57. Bolles, R. C.; Duncan, P. M., Daily course of activity and subcutaneous body temperature in hungry and thirsty rats. *Physiol Behav* **1969,** *4* (1), 87-89.
58. Shido, O.; Sakurada, S.; Kohda, W.; Nagasaka, T., Day—Night changes of body temperature and feeding activity in heat-acclimated rats. *Physiol. Behav.* **1994,** *55* (5), 935-939.
59. Werner, J.; Buse, M., Temperature profiles with respect to inhomogeneity and geometry of the human body. *J. Appl. Physiol.* **1988,** *65* (3), 1110-1118.
60. Montgomery, L. D.; Williams, B. A., Effect of ambient temperature on the thermal profile of the human forearm, hand, and fingers. *Ann Biomed Eng* **1976,** *4* (3), 209-219.
61. Hou, Y.; Matthews, A. R.; Smitherman, A. M.; Bulick, A. S.; Hahn, M. S.; Hou, H.; Han, A.; Grunlan, M. A., Thermoresponsive nanocomposite hydrogels with cell-releasing behavior. *Biomaterials* **2008,** *29* (22), 3175-3184.
62. Dong, P.; Ko, B. S.; Lomeli, K. A.; Clark, E. C.; McShane, M. J.; Grunlan, M. A., A glucose biosensor based on phosphorescence lifetime sensing and a thermoresponsive membrane. *Macromol. Rapid Commun.* **2022**, e2100902.
63. Wu, S.; Zhang, X.; Sun, Y.; Yang, H.; Lin, B.; Han, X.; Chen, P., Study on the influence of crosslinking density and free polysiloxan chain length on oxygen permeability and hydrophilicity of multicomponent silicone hydrogels. *Colloid Polym. Sci.* **2021**.
64. Wu, B.; Wiseman, M. E.; Seitz, M. E.; Tomić, K.; Heise, A.; Brougham, D. F.; Litvinov, V. M., Impact of morphology on O_2 permeability in silicone hydrogel membranes: new insights into domain percolation from experiments and simulations. *J. Membr. Sci.* **2021,** *621*, 118970.
65. Lamberti, A.; Marasso, S. L.; Cocuzza, M., PDMS membranes with tunable gas permeability for microfluidic applications. *RSC Adv.* **2014,** *4* (106), 61415-61419.
66. Caló, E.; Khutoryanskiy, V. V., Biomedical applications of hydrogels: A review of patents and commercial products. *Eur. Polym. J.* **2015,** *65*, 252-267.
67. Jacob, J. T., Biocompatibility in the development of silicone-hydrogel lenses. *Eye & Contact Lens* **2013,** *39* (1).
68. Keir, N.; Jones, L., Wettability and Silicone Hydrogel Lenses: A Review. *Eye & Contact Lense* **2013,** *39* (1), 100-108.
69. Unruh, R. M.; Bornhoeft, L. R.; Nichols, S. P.; Wisniewski, N. A.; McShane, M. J., Inorganic–organic interpenetrating network hydrogels as tissue-integrating luminescent implants: physicochemical characterization and preclinical evaluation. *Macromol. Biosci.*

2022, *22* (3), 2100380.
70. Frassica, M. T.; Jones, S. K.; Diaz-Rodriguez, P.; Hahn, M. S.; Grunlan, M. A., Incorporation of a silicon-based polymer to PEG-DA templated hydrogel scaffolds for bioactivity and osteoinductivity. *Acta Biomater.* **2019,** *99*, 100-109.
71. Munoz-Pinto, D. J.; Grigoryan, B.; Long, J.; Grunlan, M.; Hahn, M. S., An approach for assessing hydrogel hydrophobicity. *J. Biomed. Mater. Res. A* **2012,** *100* (10), 2855-2860.
72. Fei, R.; Means, A. K.; Abraham, A. A.; Locke, A. K.; Coté, G. L.; Grunlan, M. A., Self-Cleaning, thermoresponsive P(NIPAAm-co-AMPS) double network membranes for implanted glucose biosensors. *Macromolecular Materials and Engineering* **2016,** *301* (8), 935-943.
73. Dong, P.; Schott, B. J.; Means, A. K.; Grunlan, M. A., Comb architecture to control the selective diffusivity of a double network hydrogel. *ACS Appl. Polym. Mater.* **2020,** *2* (11), 5269-5277.
74. Swinehart, D. F., The beer-lambert law. *J. Chem. Educ.* **1962,** *39* (7), 333.
75. Feil, H.; Bae, Y. H.; Feijen, J.; Kim, S. W., Effect of comonomer hydrophilicity and ionization on the lower critical solution temperature of N-isopropylacrylamide copolymers. *Macromolecules* **1993,** *26* (10), 2496-2500.
76. Erbil, C.; Aras, S.; Uyanik, N., Investigation of the effect of type and concentration of ionizable comonomer on the collapse behavior of N-isopropylacrylamide copolymer gels in water. *J. Polym. Sci. A. Polym. Chem.* **1999,** *37* (12), 1847-1855.
77. Sharkawy, A. A.; Klitzman, B.; Truskey, G. A.; Reichert, W. M., Engineering the tissue which encapsulates subcutaneous implants. I. Diffusion properties. *J. Biomed. Mater. Res.* **1997,** *37* (3), 401-412.
78. Arima, Y.; Iwata, H., Effect of wettability and surface functional groups on protein adsorption and cell adhesion using well-defined mixed self-assembled monolayers. *Biomaterials* **2007,** *28* (20), 3074-3082.